LHCb Collaboration

LHCb 2001-041 VELO
25th May 2001

The performance of the SCT128A ASIC when reading out irradiated and non–irradiated VELO prototype detectors

M. Charles [1] J. Buytaert [2] J. Libby [2]

Abstract

The measurement of the SCT128A ASIC pulse shape when reading out non-irradiated and irradiated prototype detectors for the LHCb VELO is presented. The detectors studied were non–irradiated and irradiated n–on–n PR01 prototype detectors fabricated by Hamamatsu, and an irradiated p–on–n PR02 prototype detector fabricated by MICRON. The rise and optimal readout times were measured for these detectors, where the rise time is defined as the time for the response to rise from 10% of its maximum value to 90%, and the optimal sampling time is the time at which the response is maximised given the constraints that the underspill and overspill fractions at -25 ns and +25 ns respectively be 30% or less.

[1]Department of Nuclear and Particle Physics, Oxford University, 1 Keble Road, Oxford OX1 3RH, England

[2]CERN, CH-1211, Geneva 23, Switzerland

1 Introduction

This note presents the measurements of the SCT128A [1] ASIC (Application–Specific Integrated Circuit) performance when reading out irradiated and non–irradiated silicon micro–strip detectors. A modified design of the SCT128A ASIC, which will meet the level–0 electronics requirements of LHCb [2], is a possible choice for the read out of the LHCb VELO. The main modification will be the change in the multiplexing from 128:1 to 32:1. The front–end amplifier will also change leading to a slightly lower gain and reduced overspill. More details of these modifications can be found in [3].

The principal measurements are the determination of the rise time and the optimal sampling time of the output of the SCT128A. The optimal sampling point is not simply that at which the signal is maximal, it is also constrained by the signal remaining after 25 ns, the time between LHC bunch crossings. To determine these times the output signal shape of the SCT128A as a function of time is measured. In this note measurements of the signal shape were made for three different detector types: non–irradiated n–on–n, irradiated n–on–n and irradiated p–on–n. The variation in performance between SCT128A chips has also been determined for the signal shape and the gain of the ASIC. These measurements complement those presented in [4], which describes a similar analysis performed with less data.

The data used for this study were collected in August 2000 in a test–beam of 120 GeV pions and muons at the CERN SPS. Three detectors were equipped with SCT128A readout electronics: a non–irradiated Hamamatsu 1998 PR01 prototype R–measuring detector, an irradiated Hamamatsu 1998 PR01 prototype ϕ–measuring detector (maximum dose 4×10^{14} protons/cm^2) and an irradiated MICRON 2000 PR02 prototype ϕ–measuring detector (maximum dose 10^{15} protons/cm^2). The Hamamatsu detectors are n–on–n type and the MICRON detector is p–on–n type. Descriptions of these detectors, their irradiation and the test–beam layout are given in [5, 6, 7].

The organisation of this note is as follows. In Section 2 the analysis of the non–irradiated n–on–n detector is described. This detector is referred to as the fast–station throughout the remainder of this note. The geometry of the detector is briefly described before the alignment, track selection and analysis procedure are discussed. The parameterisation and fitting of the pulse shape are described and the results for the fast–station are given in Section 3. The results for the irradiated Hamamatsu and MICRON detectors are presented in Sections 4 and 5 respectively. The results are discussed and conclusions given in Sections 6 and 7.

2 Analysis of the fast–station

Firstly a description of the geometry and readout electronics of the fast–station are presented in Sections 2.1 and 2.2 respectively. The alignment of the detector is discussed in Section 2.2. The data used and the track selection is described in Section 2.4. The measurement of SCT128A output signal as a function of time is presented in Section 2.5.

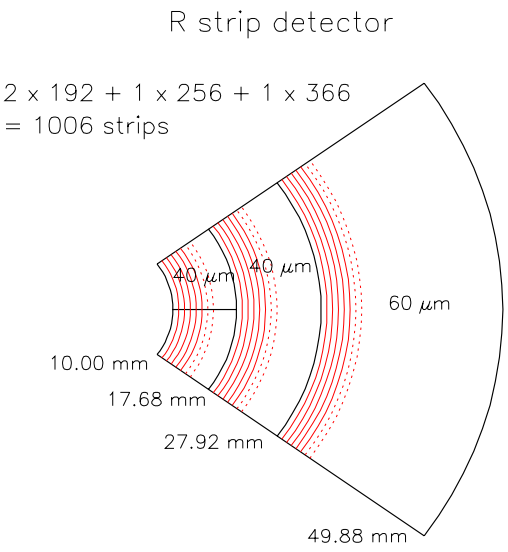

Figure 1: The strip layout of the Hamamatsu prototype R–measuring detector.

2.1 Detector geometry

The fast–station is a PR–01 (PRototype–01) series R–measuring detector[1] produced in 1998 by Hamamatsu; the design is shown in Figure 1. The silicon type is n–on–n, with a thickness of 300 μm. The detector is divided into four regions. The 3 regions at radius less than 28 mm have strips with a pitch of 40 μm. The region at a radius greater than 28 mm has strips with a pitch of 60 μm. The radial coverage of the detector is 10 mm $\leq$ R $\leq$ 50 mm, and the angular coverage is 72°.

2.2 Readout electronics

The fast–station was equipped with a 6 SCT128A hybrid. The bond pads of the detector are pitched at 50 μm (in two staggered rows of 100 μm pitch) while the hybrid inputs are pitched at 80 μm. Therefore, a dedicated fan–in was fabricated to route the signals from the detector to the hybrid. Furthermore, the fan–in was designed to readout all channels from the 40 μm pitch region of the detector. A photograph of the detector, fan–in and hybrid is shown in Figure 2. The triggering and timing of the SCT128A readout is described in [5].

2.3 Alignment

The alignment procedure of the fast–station was identical to that used in the analyses of charge collection efficiency and cluster shape presented in [5, 6]. The residuals between the extrapolated track and the cluster centre after alignment are shown in Figure 3(a). The width of the distribution was 13 μm. The residuals as a function of the local R

[1]Reference number h-R10 [8].

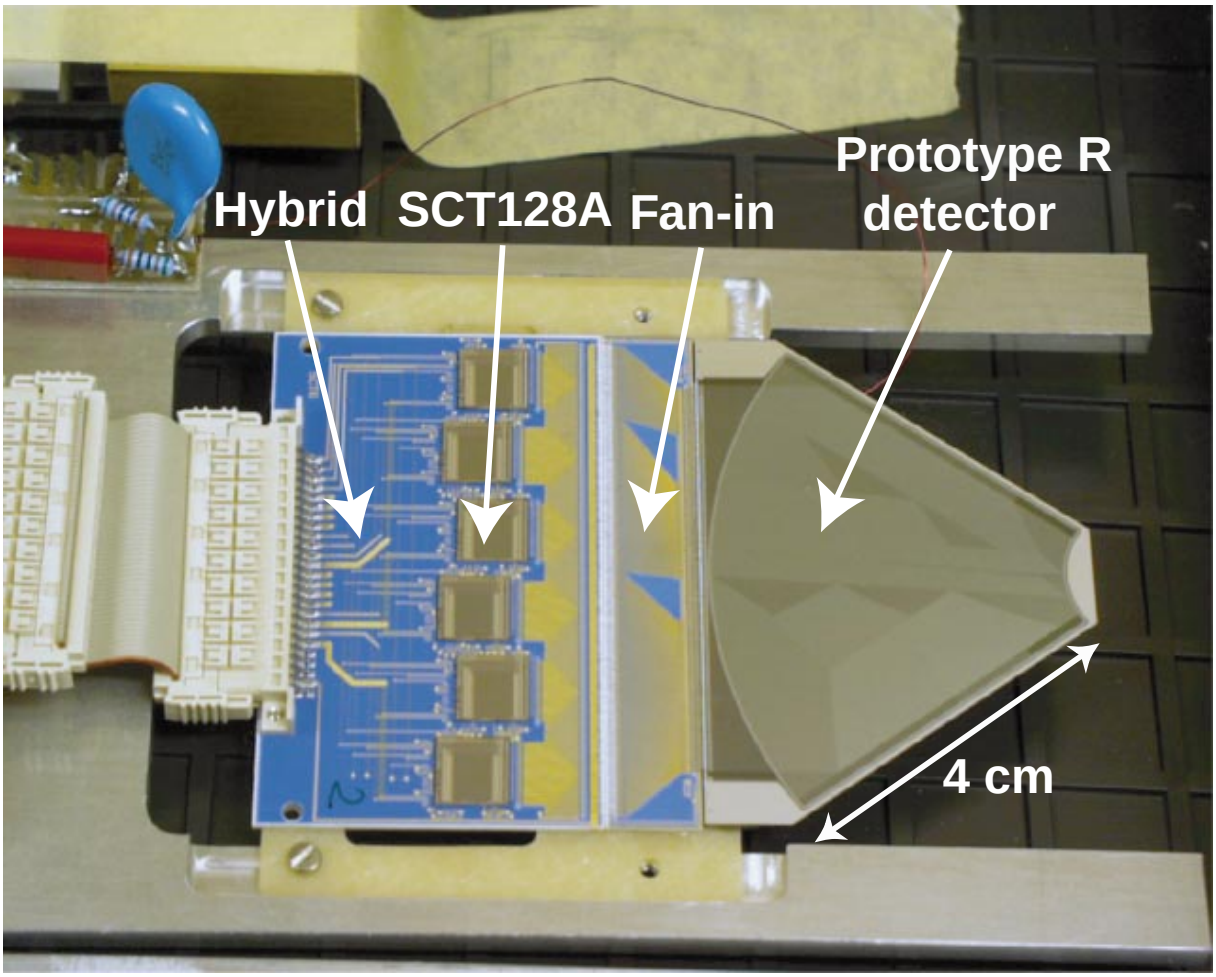

Figure 2: A photograph of the fast–station. The different components are labelled.

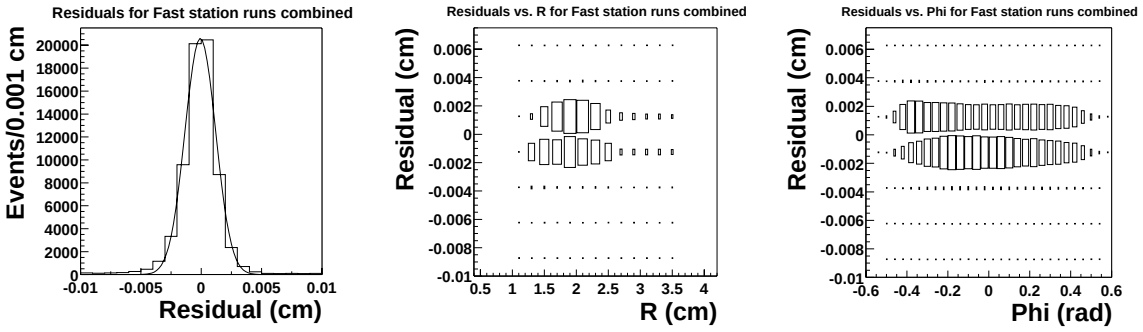

(a) (b) (c)

Figure 3: The alignment of the fast–station: (a) the residual distribution of width 13μm, (b) the residuals as a function of R, and (c) the residuals as a function of ϕ.

and ϕ positions on the detector are shown in Figures 3(b) and (c) respectively. The distribution as a function of ϕ is not flat therefore the alignment is not optimal, however it is satisfactory for the analysis presented here.

2.4 Data and track selection

Data from 99 runs were included in the analysis the numbers of which are given in the first column of Table 1. Events were only used from these runs if there was a single track reconstructed in the event with hits on all eight VA2-equipped telescope detectors. Fast–station events which would have used data from dead, noisy or unbonded strips (of which there were approximately 67) were removed from the analysis. The number of tracks selected in each set of runs is shown in Table 1. The total number of tracks selected was 145,376. The local intercept position of these tracks on the fast–station is shown in Figure 4. The hole in the coverage of SCT128A 1 is due to a concentration of dead and noisy strips.

2.5 Measurement of the signal as a function of time

To extract the pulse shape the signal must be measured over a range of times. The timing configuration of the test–beam trigger was such that a trigger was only accepted if it fell in a window of 75 or 100 ns in length [5]. The trigger windows for the runs used in this analysis are given in the third column of Table 1. The relative time of the beam trigger with respect to this window was recorded with a TDC [5].

To extract the signal a reconstructed track was extrapolated to the fast–station and the charge around the intercept point was evaluated. The charge was summed over five strips centred on the intercept point.

The measured signal in the fast–station as a function of TDC time is shown in Figure 5 for all runs. The pulse of the SCT128A can be seen clearly. Some of the runs were offset in time from one other because of tuning of time-sampling parameters during data-taking and recabling. Individual distributions were fitted with the pulse shape and the positions in TDC time at which the pulse began[2] (t_0) were aligned to give the combined plot. The offsets used are given in column four of Table 1. The changes in the TDC time window lead to some intervals of TDC time having greater statistics than others.

3 Results from the fast–station

The method for extracting the pulse shape is described in Section 3.1. The results for the fast–station are presented in Section 3.2 and the uncertainties on these results is discussed in Sections 3.3 and 3.4.

3.1 Method

To determine the most probable value of the signal at a given time interval, a suitable function was fitted to the charge distribution using a log-likelihood method. If the charge distribution was noise–dominated (values close to zero) the function used was a Gaussian,

[2]Defined in Section 3.1.

Run numbers	Tracks selected	Trigger window [ns]	Relative offset [ns]
2595-2596	4830	100.0	-21.3
2597-2618	42114	100.0	0.0
2621-2639	18319	100.0	0.0
2642-2649	6146	100.0	0.0
2651-2655	3762	100.0	0.0
2667-2679	7150	100.0	0.0
2875-2878	7637	75.0	-55.9
2918-2921	8654	75.0	-55.9
2928-2931	7000	75.0	-55.9
2943-2946	6878	75.0	-55.9
2999-3004	14482	75.0	-55.9
3034-3038	11172	75.0	-55.9
3059-3061	7232	75.0	-55.9

Table 1: The runs used in the analysis of the fast–station. The number of tracks reconstructed, the duration of the trigger window and the relative time offset used are given, as described in Section 2.5. The three different offset groups cover the central and tail regions (-21.3 ns), the rise and central regions (0.0 ns) and the central region (-55.9 ns) of TDC time shown in Figure 5.

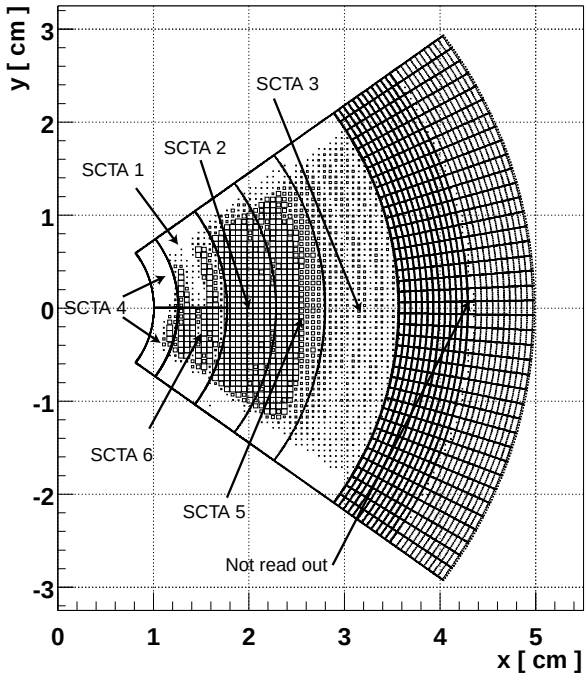

Figure 4: The overlap of the tracks used in the analysis with the fast–station. The regions read out by different SCT128As and the region not equipped with readout electronics are indicated.

otherwise for signal–dominated distributions a pseudo-Landau was used. Intervals were considered to be noise–dominated if their modal bin centre lay within 9 ADC counts of zero; this cut value was chosen because it minimised the χ^2/NDF[3] values of the fits to the charge distributions at the transition between the noise– and signal–dominated regions. This strategy is similar to that used in [4].

The pseudo-Landau function used here was a symmetrised version of Moyal's approximation to the Landau distribution [9], given by:

$$\begin{aligned} f(x) &\propto e^{-(v(x)+e^{-v(x)})/2} \text{ , and} \\ v(x) &= |x - x_0|/w_{\pm} \text{ ,} \end{aligned}$$

where x is the charge in ADC counts, x_0 is the most probable ADC value and w is the width. Different width values w_+ and w_- are used for $x > x_0$ and $x < x_0$ respectively. The value of $w_{\pm}$ is constrained to be positive. The Gaussian fits give x_0 and a single width, σ.

This differs from the function used in other analyses of the SCT128A pulse shape [4], and for the analyses of charge collection efficiency and cluster shape of the irradiated detectors [5, 6], which have:

$$v(x) = (x - x_0)/w_{\pm} \text{ .}$$

The systematic error arising from the parameterisation of the pseudo–Landau distribution is given in Section 3.3.

The fits were performed to charge distributions integrated over 2 ns TDC time intervals. Six example charge distribution fits are shown in Figure 6. The parameters extracted from all the fits as a function of TDC time are shown in Figure 7 along with the χ^2/NDF of the fit.

The pulse shape is then extracted from the distribution of most probable values as a function of TDC time distribution. The approximated function, $o(t)$, used to describe the SCT128A output signal as a function of time is described in [4] and the references therein. The approximated SCT128A signal shape depends on 7 parameters; 3 describe the input signal from the silicon as a function of time and 4 describe the response of the SCT128A.

The input signal shape is parameterised as a flat–topped pulse with linear front and back edges. The parameters are the rise time of the front–edge, t_{rise}, the duration of the flat top, t_{plat}, and the fall time of the back edge, t_{fall}. The four parameters which describe the SCT128A response are the time at which the output signal begins, t_0, two frequency poles a and b and the signal normalisation, $norm$. The parameters $norm$, a and b are correlated with the parameters describing the input signal; this complicates the interpretation of the fitted values as the true signal shape from the silicon sensor.

The fitted pulse shape to all the fast–station data analysed is shown in Figure 8; the χ^2/NDF of the fit was 1.9.

3.2 Results of pulse shape fit

The time at which the signal is maximal after t_0, τ_{max}, was extracted numerically from the fitted function. A numerical rather than an analytical method was used because of the function's complexity.

[3] NDF=Number of Degrees of Freedom.

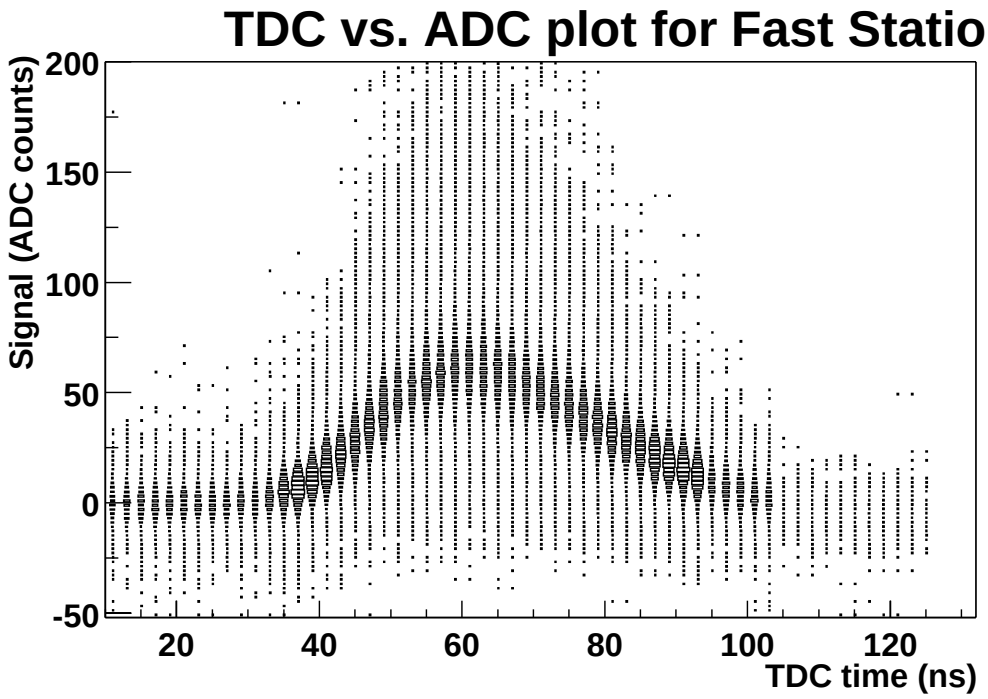

Figure 5: The signal in the fast–station as a function of TDC time for all the data used in the analysis.

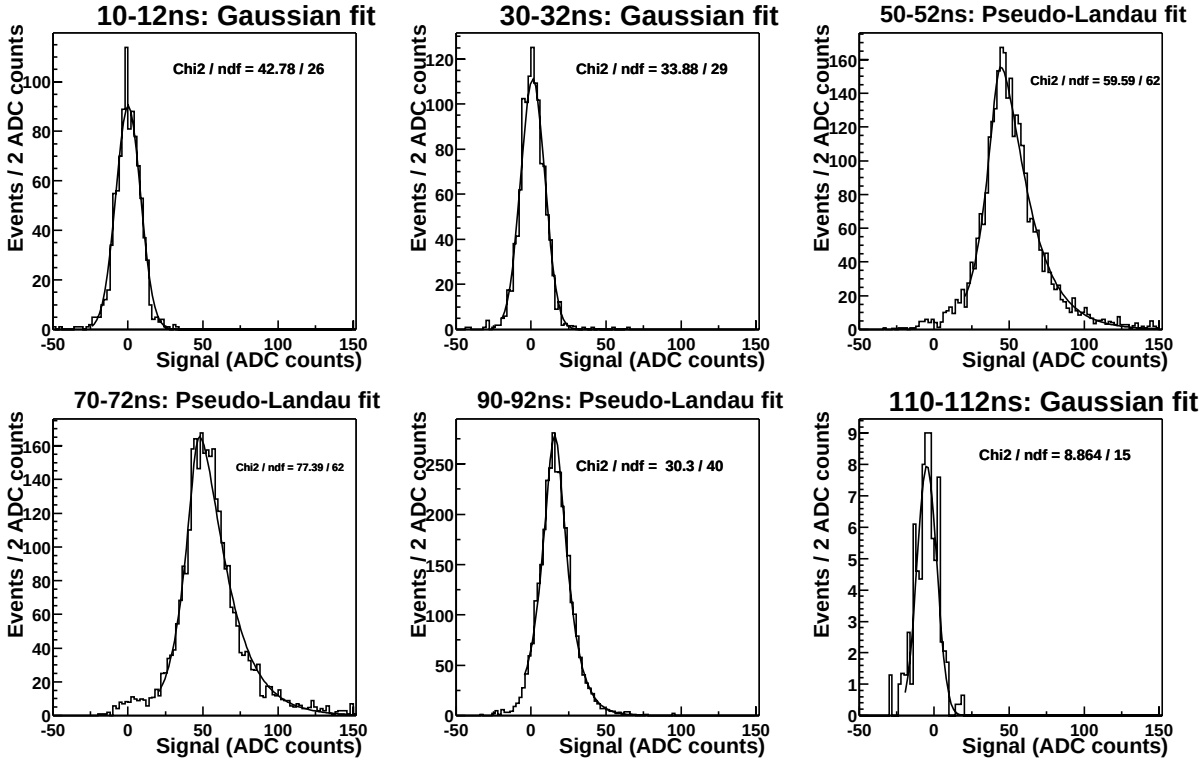

Figure 6: Pseudo-Landau and Gaussian fits to the signal distribution of the fast–station for 6 different TDC time intervals.

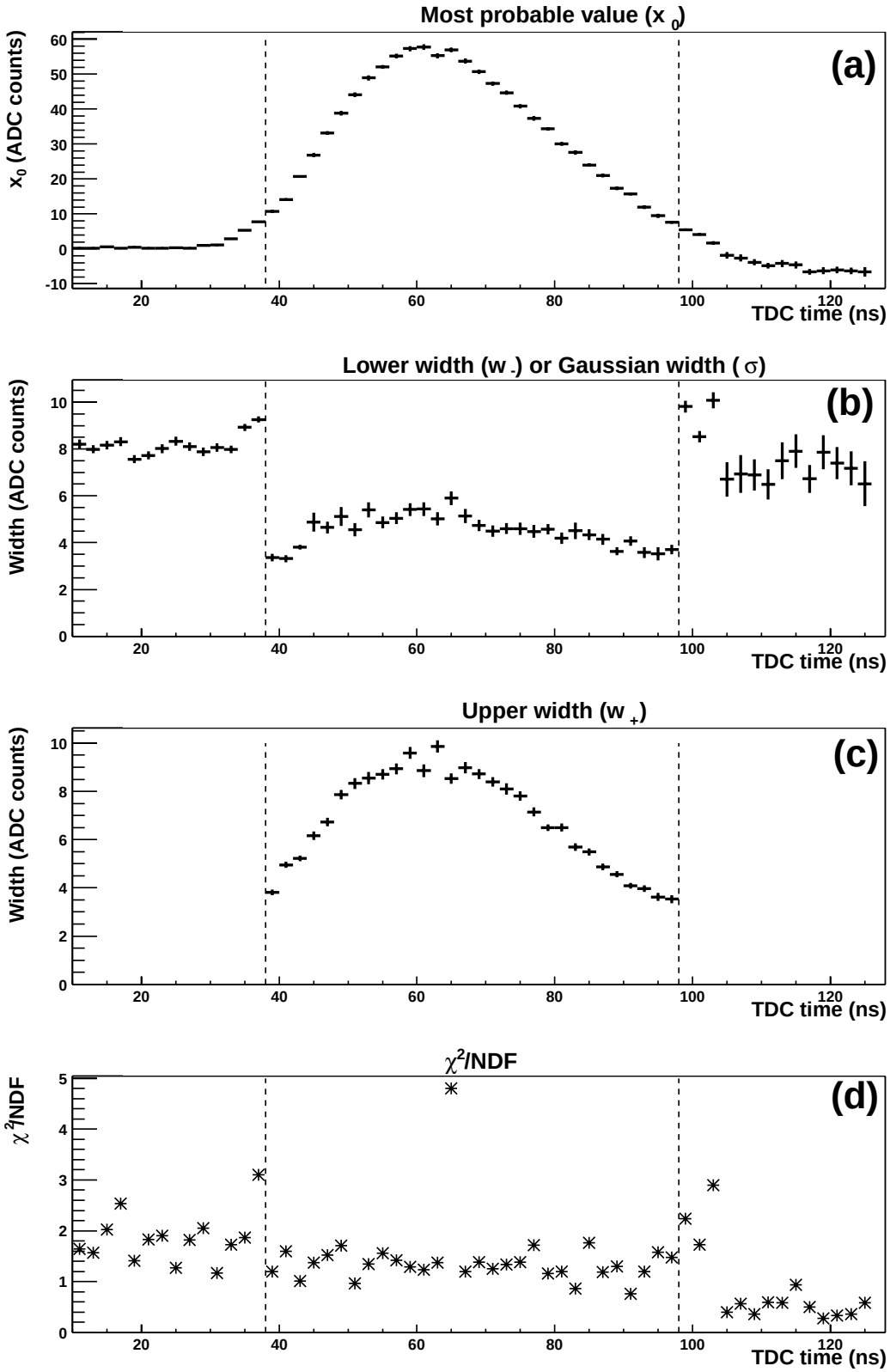

Figure 7: The values of (a) x_0, (b) σ (Gaussian) or w_- (pseudo–Landau) and (c) w_+ fitted to charge distributions integrated over 2 ns TDC time intervals as function of the TDC time. The χ^2/NDF of the fits are also given in (d). The region between the dashed lines (38 ns–98 ns) is signal–dominated and the rest is noise–dominated.

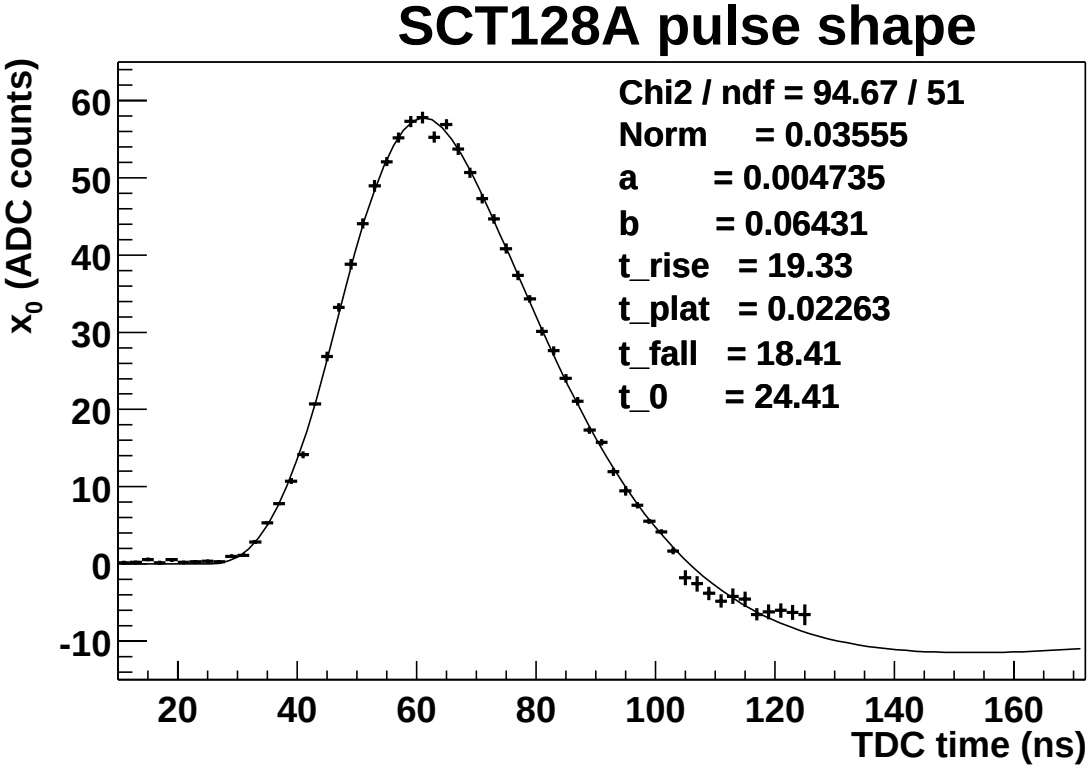

Figure 8: The fit to the signal shape for the fast–station.

The value of τ_{max} for the fast–station was found to be:

$$\boldsymbol{\tau_{max} = 36.8 \text{ ns after } t_0 \ .}$$

The maximum signal $o(\tau_{max})$ is 58 ADC counts, and the overspill fraction—the fraction of the amplitude remaining after 25 ns—at the peak is 38%. The quantities $\tau_{10\%}$ and $\tau_{90\%}$—the times at which the signal is at 10% and 90% of the $o(\tau_{max})$ respectively—were also determined; it was found that the rise time, defined as $\tau_{rise} \equiv \tau_{90\%} - \tau_{10\%}$, was:

$$\boldsymbol{\tau_{rise} = 19.1 \text{ ns} \ .}$$

3.2.1 Optimal sampling time

Two factors must be considered when determining the sampling time: maximising the signal and minimising the overspill into the next sampling point 25 ns later. It has been estimated that the overspill fraction must be 30% or less not to degrade the level–1 trigger performance [10]. Therefore, the optimal sampling point, τ_{opti}, is defined as the time after t_0 at which the signal is maximised given the constraints that:

$$\begin{aligned} \frac{o(\tau_{opti} - 25 \text{ ns})}{o(\tau_{opti})} &< 30\% \text{ , and} \\ \frac{o(\tau_{opti} + 25 \text{ ns})}{o(\tau_{opti})} &< 30\% \ . \end{aligned}$$

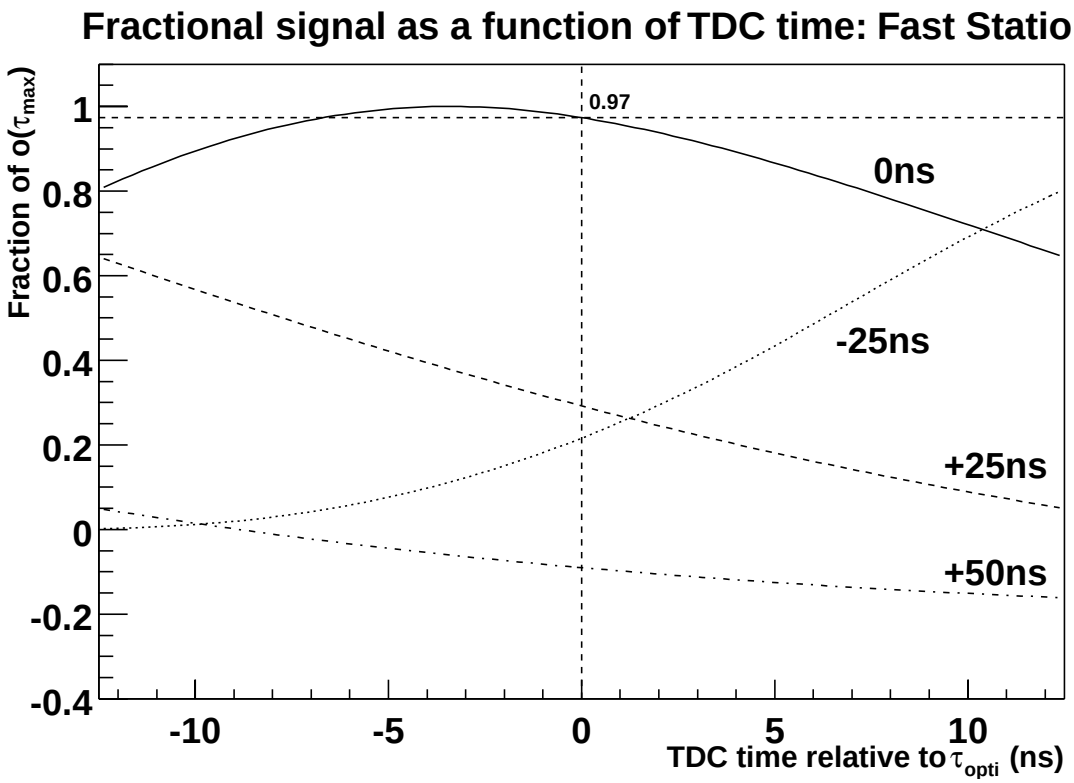

Figure 9: The signal fraction as a function of time relative to the optimal sampling point for the fast–station. The signal (solid line), underspill by 25 ns (dotted line), and overspill by 25 ns and 50 ns (dashed and dot–dashed lines) are shown.

For the fast–station this was found to be:

$$\boldsymbol{\tau_{opti} = \tau_{max} + 3.4 \text{ ns} = 40.2 \text{ ns after } t_0 \ .}$$

The fraction of the maximum signal at τ_{opti} is 97%. In addition, the time after τ_{max} at which the signal should be sampled, $\Delta\tau_{opti} \equiv \tau_{opti} - \tau_{max}$, is defined. $\Delta\tau_{opti}$ is 3.4 ns for the fast–station.

Figure 9 shows the signal, underspill by 25 ns and overspill by 25 ns and 50 ns calculated using the pulse shape functions fitted to the data with respect to the optimal sampling point. The rise is clearly steeper than the fall after the peak; it is because of this that τ_{opti} is after the peak rather than before it. The functions are normalised to the maximum signal observed and the time is taken relative to τ_{opti}.

3.3 Statistical errors

The combined number of events from the fast–station is large, so the statistical errors are expected to be relatively small. Final values for these errors have not yet been determined because of two problems:

- The correlation matrix has not yet been extracted from the χ^2 fitting process; because of the correlation between parameters their uncertainties cannot be interpreted without it.

SCT128As	Events	τ_{max} [ns]	$o(\tau_{max})$ [ADC]	τ_{opti} [ns]	$\Delta\tau_{opti}$ [ns]	$\frac{o(\tau_{opti})}{o(\tau_{max})}$ [ns]	τ_{rise} [ns]	χ^2/NDF
All (1–6)	145376	36.8	57.8	40.2	3.4	0.97	19.1	1.9
1,2,4,5,6	120683	36.3	59.3	40.0	3.7	0.97	18.8	2.0
1	5546	35.1	60.5	37.6	2.5	0.99	18.4	1.5
2	60399	36.2	62.1	39.4	3.2	0.97	19.9	1.1
3	24693	34.7	47.6	37.9	3.3	0.99	18.0	1.0
4	1454	33.1	58.3	33.1	0.0	1.00	17.4	2.9
5	42871	37.2	57.7	41.7	4.5	0.96	19.2	1.4
6	10413	33.8	57.6	39.3	5.5	0.94	17.3	1.4

Table 2: Results of the signal shape parameters for each SCT128A on the fast–station. In addition, the combined results with and without SCT128A 3 are given.

- The quantities being determined are not fitted directly but calculated from the parameters. Currently this is being done numerically because of the complexity of the pulse shape function; an analytic relation between their errors and those of the parameters has not yet been determined.

3.3.1 SCT128A-by-SCT128A variation

The data were divided into six samples corresponding to which SCT128A was used in the readout. The pulse shapes from the six SCT128As read out are shown in Figure 10. The number of events in each SCT128A, the fitted parameters and the χ^2/NDF are given in Table 2; the combined results are also given for comparison. As can be seen, the statistics for SCT128A 4 are not sufficient for a reliable fit and the maximum value in SCT128A 3 is 18% lower than in the others, however the timing properties are compatible with the other SCT128As.

A possible cause of the lower gain in SCT128A 3 is a greater input load capacitance compared to the other SCT128As [3]. The longest strips, which have a capacitance of ~ 22 pF [11], are those read out by SCT128A 3. However, for the range of capacitances (15–22 pF) of the strips read out on the fast–station, the SCT128A response is expected to vary by 4% at most; therefore, the 20% less gain observed in SCT128A 3 can not be attributed to this. A more detailed study of the gain of SCT128A and SCTA_VELO response with input load capacitance will be performed in the future (see Section 7).

A statistical analysis of the results from the SCT128As was performed. Working from the assumptions that they were independent and directly compatible, statistical errors on the weighted means of the quantities were calculated. These errors are shown in Table 3.

3.4 Systematic errors

3.4.1 Alignment in TDC time

As discussed in Section 2.5, there was a relative offset between different batches of runs. This was measured by comparing the fitted t_0 parameter with runs 2597–2679. The timing of the runs was then adjusted to correct for this offset; after this, the fitted t_0 values were found to be consistent within their uncertainties. From comparisons of the fits to the

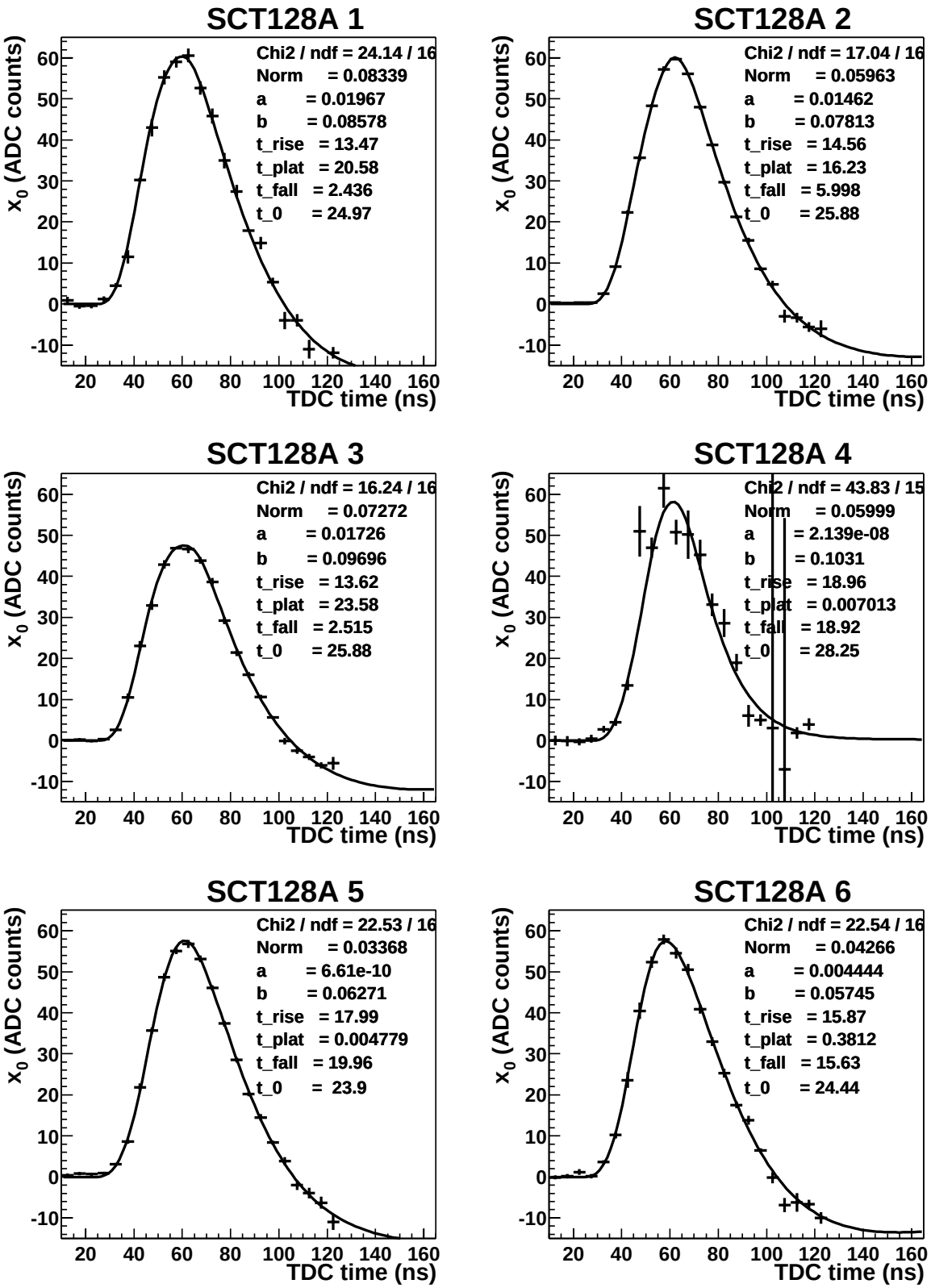

Figure 10: The fit to the signal shape for individual SCT128As on the fast–station.

Source of uncertainty	τ_{max} [ns]	$o(\tau_{max})$ [ADC]	τ_{opti} [ns]	$\Delta\tau_{opti}$ [ns]	$\frac{o(\tau_{opti})}{o(\tau_{max})}$	τ_{rise} [ns]
Statistical	0.5	2.3	0.7	0.4	0.6%	0.4
Alignment in TDC time	0.9	0.7	0.4	0.6	1.0%	0.2
Number of strips	0.3	1.1	0.1	0.1	0.2%	0.2
Gaussian cut-off	0.2	0.1	0.4	0.3	0.4%	0.2
Choice of pseudo-Landau	1.4	5.6	0.6	0.8	1.1%	0.1
$\Rightarrow$ Sum of systematics	1.8	6.2	1.1	1.1	1.7%	0.5

Table 3: Statistical and systematic uncertainties on the derived quantities.

three batches, systematic errors from combining data at different offsets were estimated and are given in Table 3.

Note that the values of τ_{max} and τ_{opti} are both defined relative to t_0, so the results are dependent on the quality of the fit at the beginning of the pulse. An example of this can be found in the discussion of pseudo-Landau functions in Section 3.4.2. The quantity $(\tau_{opti} - \tau_{10\%})$ can be used as a cross check that the uncertainties are not dominated by this, since it is less sensitive to the offset t_0 and more sensitive to the shape of the pulse. The errors on it are found to be slightly smaller than those on τ_{opti}, but of the same order (0.4 ns vs. 0.7 ns statistical and 0.9 ns vs. 1.1 ns systematic for $(\tau_{opti} - \tau_{10\%})$ and τ_{opti} respectively). From this it was concluded that the results do not depend significantly on the uncertainty in t_0.

3.4.2 Fitting of ADC distribution

Number of strips: When determining the signal of an event, five strips were integrated over, centred on the track intercept point. The effects of using only three strips were also considered; it was found that there was little change to the timing properties and essentially no change in the fraction of the maximum value seen at τ_{opti}. There was a decrease in the maximum value of 1.1 ADC counts, possibly due to residual misalignment to which data integrated over fewer strips is more vulnerable. These uncertainties are shown in Table 3.

Gaussian cut-off: As described in Section 3.1, there is a cut-off below which a Gaussian is used instead of a pseudo-Landau when fitting slices of TDC time. The effects on the fast–station of varying this cut-off were investigated; it was found that a change of up to 3 counts in either direction produced a small amount of deviation. This is shown in Table 3.

Choice of pseudo-Landau function: As described in Section 3.1, there is a choice of function to use for fitting the ADC distribution in slices of TDC time. The analysis was repeated with the function used in [4]; the change was found to have a significant effect on the results of the pulse shape fit, as shown in Table 3. Sample fits together with the χ^2/NDF values of its fits are shown in Figure 11. The average χ^2/NDF of these is 1.7 as compared with 1.4 for the pseudo-Landau function used in the rest of the analysis (excluding Gaussian fits from the average in both cases). The

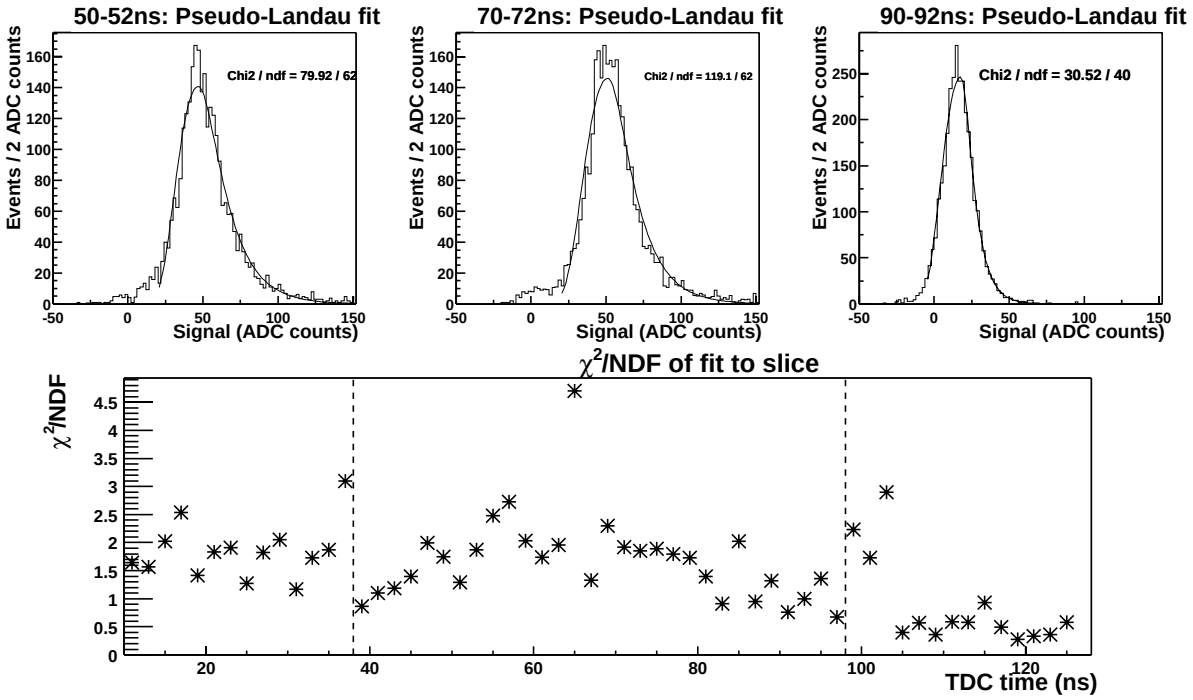

Figure 11: Sample fits to the signal distribution made using an alternative pseudo-Landau function and the χ^2/NDF values of this function.

χ^2/NDF of the pulse shape function to the most probable values extracted using the alternative pseudo-Landaus is 3.3.

The principal difference in the pulse shapes is that the alternative pseudo-Landau gives a consistently higher most probable value, raising $o(\tau_{max})$ by 5.6 ADC. The time behaviour is also different; the rise of the pulse is similar, so that the the values of τ_{rise} match to 0.1 ns. However, the values of t_0 fitted differ by 1.2 ns, so there is a corresponding offset (within 0.2 ns) of the opposite sign in the quantities defined relative to it, τ_{max} and τ_{opti}. The fall of the pulse is somewhat shallower, though, making τ_{opti} and $\Delta\tau_{opti}$ 0.8 ns later than would otherwise have been the case.

3.5 Summary

The estimates of errors made above are shown in Table 3 together with the sum in quadrature of the systematic errors. These are significantly larger than the statistical uncertainties in nearly every case, mostly due to the large contributions from the choice of pseudo-Landau. The uncertainty on τ_{rise} is the least sensitive to these systematic effects with the statistical and systematic uncertainties being nearly equal.

4 Results from the irradiated Hamamatsu prototype

A partially irradiated Hamamatsu prototype detector was tested in the test–beam setup [5]; the maximum dose recieved was 4.1×10^{14} protons/cm^2. Data were taken at five different bias voltages: 50 V, 100 V, 125 V, 180 V and 220 V. For each bias voltage, the pulse

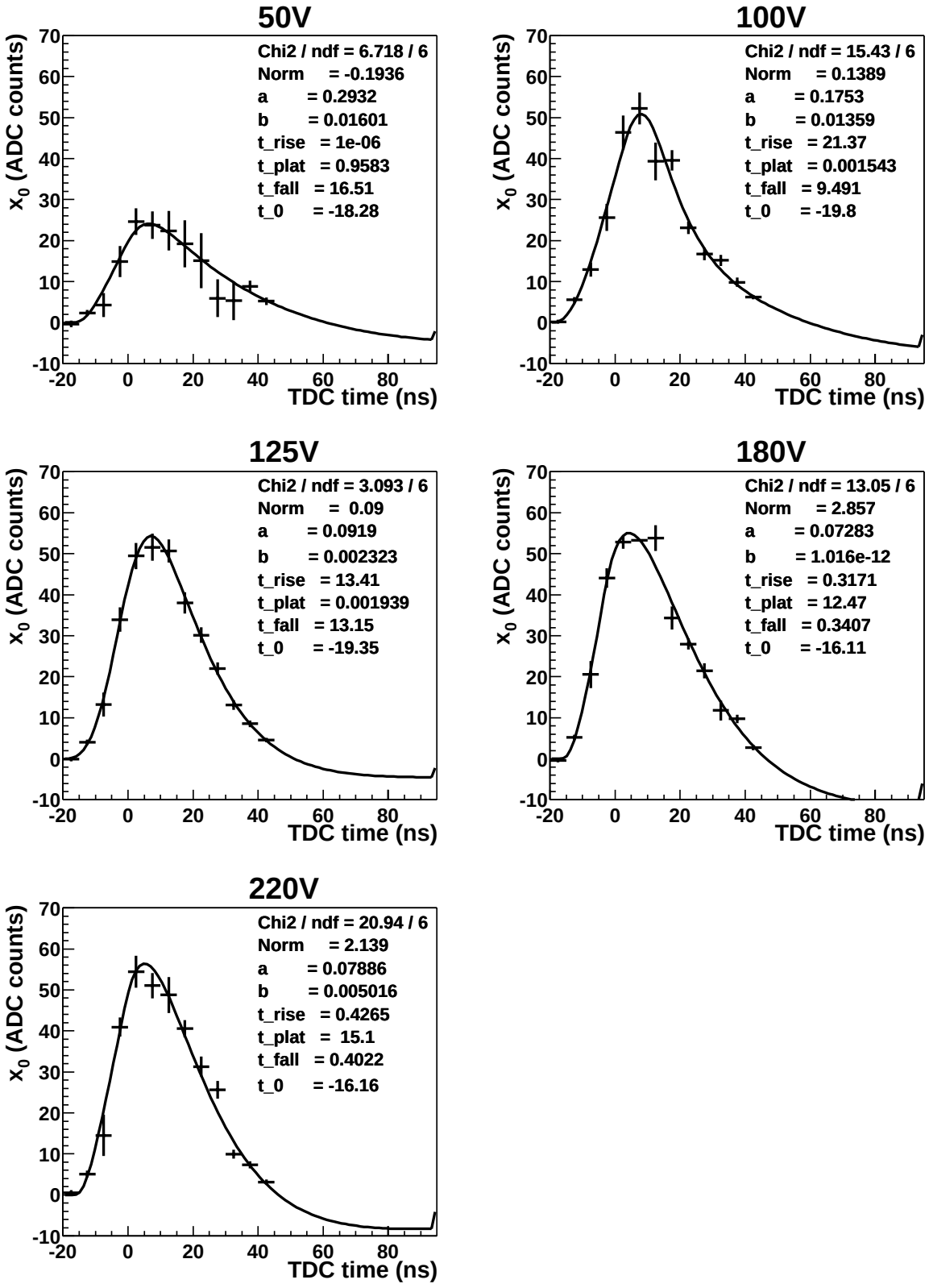

Figure 12: The fits to the signal shape for the irradiated region ($> 2.5 \times 10^{14}$ protons/cm^2) of the Hamamatsu prototype detector at five different bias voltages.

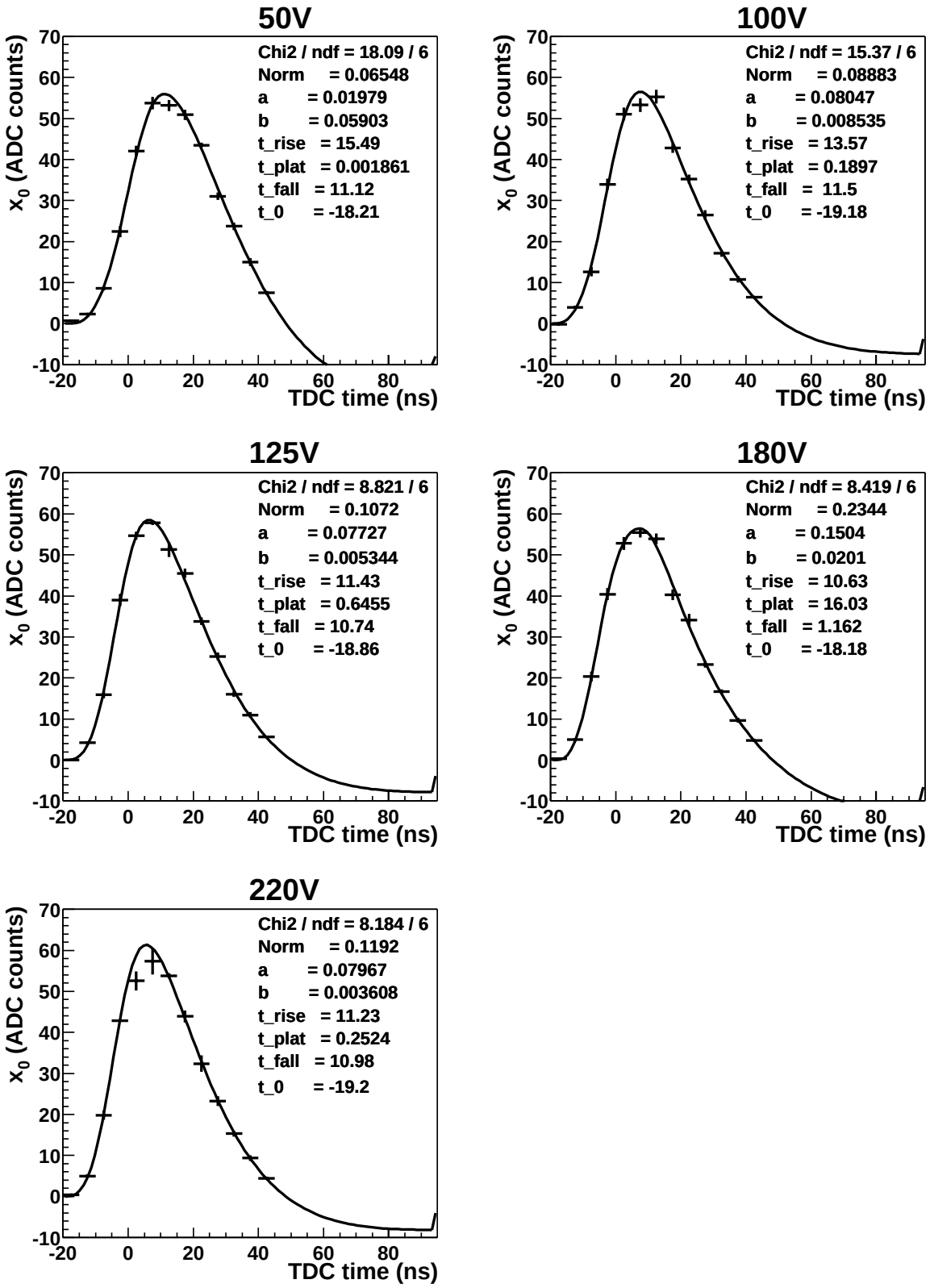

Figure 13: The fits to the signal shape for the less-irradiated region ($< 2.0 \times 10^{14}$ protons/cm^2) of the Hamamatsu prototype detector at five different bias voltages.

Voltage	Run Numbers	Events	τ_{max} [ns]	$o(\tau_{max})$ [ADC]	τ_{opti} [ns]	$\Delta\tau_{opti}$ [ns]	$\frac{o(\tau_{opti})}{o(\tau_{max})}$	τ_{rise} [ns]	χ^2/NDF
Region with fluence $< 2.0 \times 10^{14}$ protons/cm^2									
50V	2798–2801	3703	29.3	48.3	31.3	1.9	0.99	14.7	3.7
100V	2791–2793	4383	26.7	56.6	27.2	0.4	1.00	13.8	2.6
125V	2794–2797	5221	25.3	58.6	26.0	0.7	1.00	12.8	1.5
180V	2805–2809	5065	25.3	56.5	25.3	0.0	1.00	13.1	1.4
220V	2810–2814	3286	24.7	61.4	24.8	0.1	1.00	12.6	1.4
Region with fluence $> 2.5 \times 10^{14}$ protons/cm^2									
50V	2798–2801	432	24.8	23.1	35.5	10.6	0.80	13.4	6.5
100V	2791–2793	1250	27.8	50.9	27.8	0.0	1.00	16.0	2.6
125V	2794–2797	1202	26.5	54.4	26.5	0.0	1.00	13.7	0.5
180V	2805–2809	1118	20.4	55.1	21.6	1.3	1.00	11.5	2.2
220V	2810–2814	755	21.2	56.5	21.2	0.0	1.00	12.6	3.5

Table 4: Pulse shape fit results for the irradiated Hamamatsu detector in regions of different irradiation as a function of bias voltage.

shapes fitted to events from regions with an irradiation of at least 2.5×10^{14} protons/cm^2 are shown in Figure 12, and those from regions with less than 2.0×10^{14} protons/cm^2 in Figure 13. The results as a function of voltage are given in Table 4.

As reported elsewhere [5], the less irradiated region recovers full charge at a lower voltage, but the maximum signal is independent of irradiation across the detector within statistical fluctuations. Likewise, the timing behaviour appears to be similar, with large discrepancies mostly restricted to the 50V irradiated data which had poor statistics. There appears to be a decrease in τ_{opti} and τ_{rise} as the voltage increases. Such a ballistic effect in over–depleted silicon has been predicted [12]. However, there is no significance to this result within the estimated statistical uncertainty given in Section 6.

5 Results from the irradiated Micron prototype

A MICRON prototype was also studied in the same test–beam setup [6]. At present only events with tracks intercepting the inner–region, $R < 1.8$ cm in local coordinates, have been studied. Events from an irradiated region with a mean dose of 9.6×10^{14} protons/cm^2 were analysed at seven different voltages between 100 V and 390 V. Also studied was one set of data at 300 V from a non–irradiated section of the detector (mean dose $< 1 \times 10^{14}$ protons/cm^2); for more details the reader is referred to [6]. Pulse shape fits for different irradiation levels and voltages are shown in Figure 14 and the fit results are given in Table 5.

Unfortunately, there are few events from the non-irradiated part of the detector and the fit is very poor with a χ^2/NDF of 10.4. However, there are reasonable statistics in the irradiated section. The timing parameters were consistent over the range of voltages in the irradiated region.

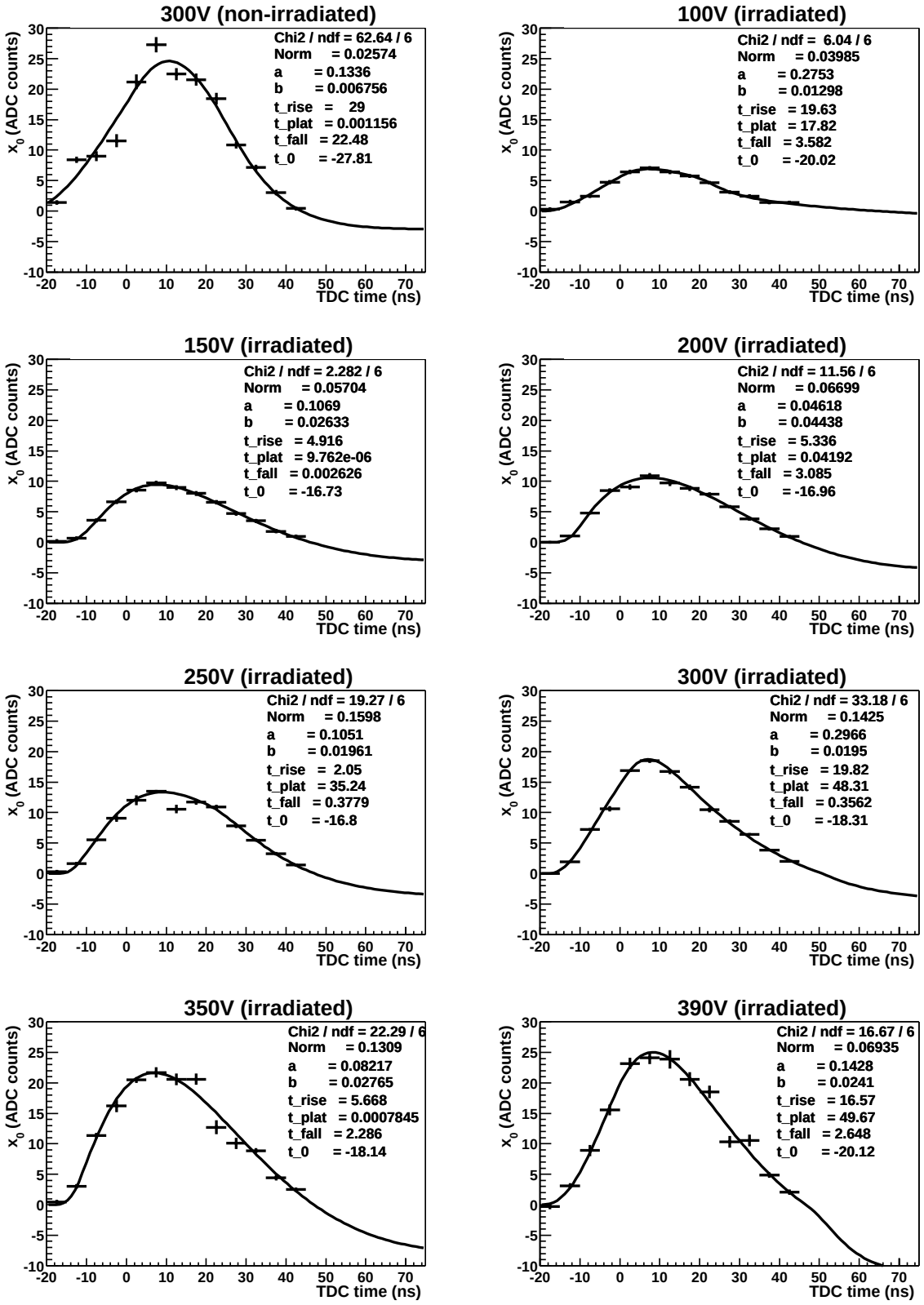

Figure 14: Fits to the signal shape for the inner region of the MICRON detector at different irradiation and bias voltage.

Voltage	Events	τ_{max} [ns]	$o(\tau_{max})$ [ADC]	τ_{opti} [ns]	$\Delta\tau_{opti}$ [ns]	$\frac{o(\tau_{opti})}{o(\tau_{max})}$	τ_{rise} [ns]	χ^2/NDF
Inner region, non-irradiated								
300V	3179	38.5	24.6	38.5	0.0	1.00	22.0	10.4
Inner region, irradiated								
100V	10053	27.3	6.9	28.8	1.5	0.99	15.8	1.0
150V	4500	24.5	9.5	26.2	1.6	0.99	13.1	0.4
200V	10414	24.5	10.6	27.1	2.6	0.99	12.7	1.9
250V	7119	25.8	13.4	27.5	1.6	1.00	14.4	3.2
300V	20364	25.4	18.8	26.5	1.2	1.00	15.2	5.5
350V	4434	25.1	21.7	28.6	3.5	0.98	13.2	3.7
390V	2791	28.3	25.1	29.1	0.7	1.00	15.3	2.8

Table 5: Pulse shape fit results for the irradiated MICRON detector in regions of different irradiation as a function of bias voltage.

6 Comparison of the three detectors

The time behaviour of most depleted data available from each of the detectors is summarised in Table 6. The non-irradiated region of the MICRON detector is not included because the fits to the data are not reliable, due to low statistics and a large χ^2/NDF. Also shown are approximate errors, obtained under the assumption that their distributions are the same as for the fast–station and adding systematic and statistical in quadrature. It should be noted that the systematics are likely to be strongly correlated between detectors. However, the irradiated detectors are dominated by statistical uncertainties. The fraction of the maximum signal as function of time, relative to τ_{opti}, for the irradiated Hamamatsu and MICRON detectors is shown in Figure 15; this can be compared to Figure 9.

As noted in Section 4, the maximum signal and timing properties extracted from fits to the irradiated and non-irradiated regions of the Hamamatsu prototype appear to be consistent within their errors at high voltage. However, those errors are currently large and more work needs to be done to investigate whether this is still the case at the level of 1–2 ns.

There is a difference between the data taken with the irradiated Hamamatsu prototype and the fast–station; τ_{max}, τ_{opti} and τ_{rise} take higher values in the fast–station by around $2-3\sigma$. This is suggestive but not conclusive; greater statistics are required. Given the apparent internal consistency of the two detectors, the most likely explanation is a systematic effect; one possibility is that the single SCT128A through which all data from the Hamamatsu prototype was read out behaved anomalously.

It is not possible to make a similar comparison for the MICRON detector because the fits to data from the non-irradiated region is poor. Results are from the irradiated region lie between the fast–station and partially irradiated Hamamatsu values, and are compatible with both.

Clearly, more data are needed, particularly from the irradiated prototypes at full depletion. There is some data collected in the outer region of the irradiated MICRON

Section of detector	τ_{max} [ns]	τ_{opti} [ns]	τ_{rise} [ns]	$\Delta\tau_{opti}$ [ns]
Fast–station Hamamatsu	36.8 ± 1.9	40.2 ± 1.3	19.1 ± 0.6	3.4 ± 1.2
Hamamatsu (non-irradiated region)	24.7 ± 3.8	24.8 ± 4.8	12.6 ± 2.7	0.1 ± 2.9
Hamamatsu (irradiated region)	21.2 ± 7.1	21.2 ± 9.8	12.6 ± 5.6	0.0 ± 5.7
MICRON (inner irradiated region)	28.3 ± 4.0	29.1 ± 5.2	15.3 ± 2.9	0.7 ± 3.1

Table 6: Pulse shape fit results summarised for the 3 detectors and different irradiation levels at the highest bias voltage recorded.

detector which was collected in the 2000 test–beam and has not yet been analysed fully. Test–beam and laboratory measurements in 2001 will provide an opportunity for more data to be taken with all three detectors.

7 Summary and conclusions

Data from the August 2000 test–beam have been analysed to determine the SCT128A pulse shapes for two 300 μm Hamamatsu detectors, one of which was partially irradiated, and a 200 μm irradiated Micron detector. The time-responses were fitted with a pulse shape function and the optimal sampling time was extracted. This was found to be 40.2 ns after the start of the pulse for the non-irradiated Hamamatsu fast–station. At this time, 97% of the maximum signal remained, with an overspill fraction of 30%. The rise time was found to be 19.1 ns.

The time behaviour appeared to be different to this for the partially irradiated Hamamatsu and Micron prototypes, with lower optimal sampling times. Similar results from regions of high and low dose on the Hamamatsu suggest that this is not a consequence of the irradiation. The uncertainties are too large for conclusions to be drawn from this data set.

7.1 Future work

The following topics will be investigated further in the coming months.

- The possibility of a discrepancy in optimal sampling times between non-irradiated and irradiated detectors must be investigated further using test–beam and laboratory measurements.
- Ballistic effects in over–depleted silicon detectors will be studied [12] and the difference in the SCT128A response with input load capacitance.
- A more detailed study of the pseudo-Landaus used to fit the signal distribution in slices of TDC time is needed; the values extracted from fits were found to be strongly dependent on which function was fitted, producing large systematic uncertainties.
- The statistical errors on derived quantities such as τ_{opti} need to be analysed in more detail, extracting the correlation matrix and relating errors on derived quantities to

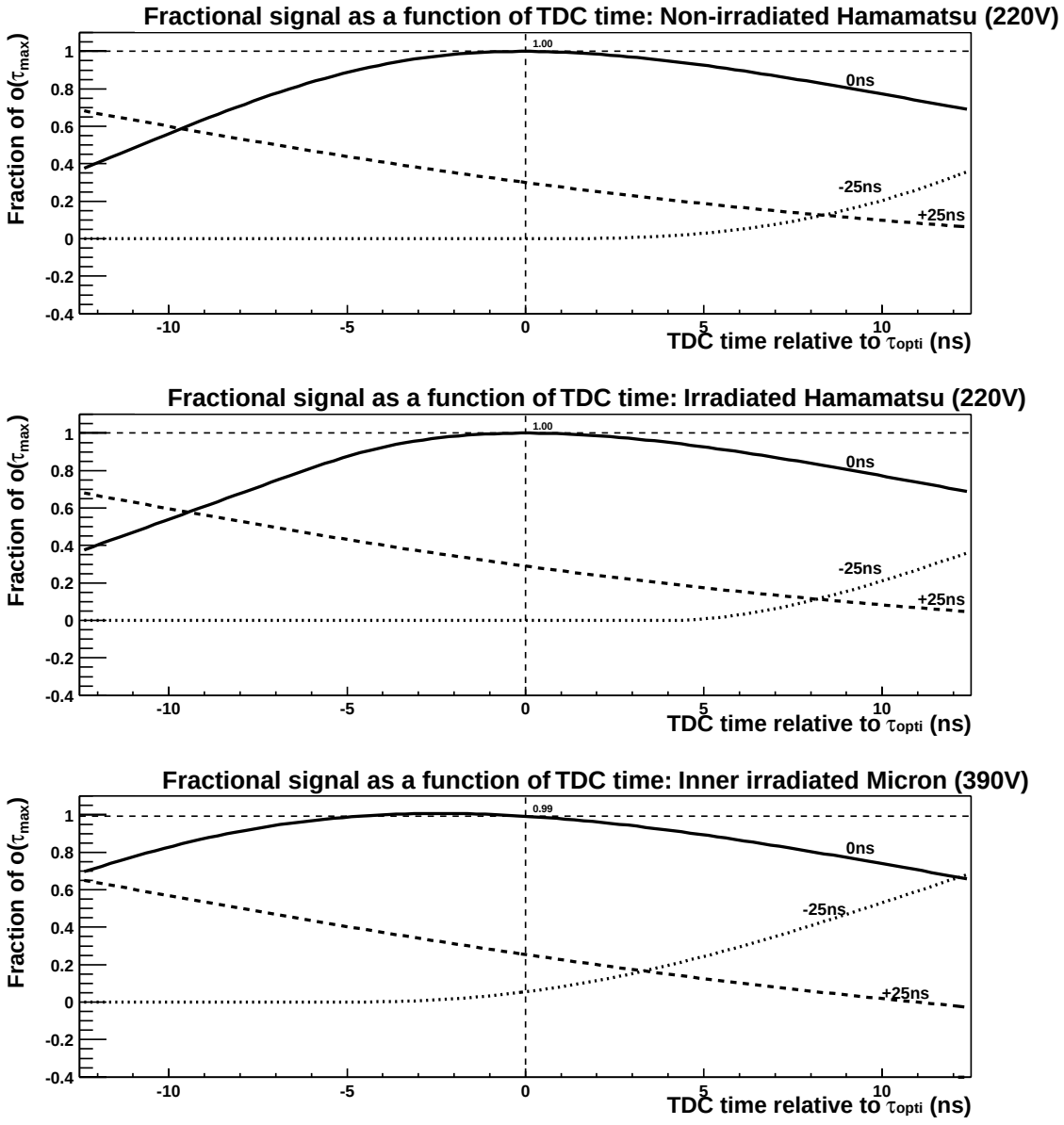

Figure 15: The signal fraction as a function of time relative to the optimal sampling point for all the irradiated and non–iraddiated regions of the Hamamatsu prototype and the MICRON prototype.

those on the fitted parameters. So far, this has not been accomplished using the current fitting procedure.

- The analysis will need to be repeated when data from the new SCTA, SCTA_VELO and Beetle [13] ASICs become available.

8 Acknowledgements

We would like to thank VELO testbeam group, in particular Paula Collins and Chris Parkes, for their help and advice. In addition, we would like to thank Lau Gatignon, Rolf Lindner and the staff of the CERN-PS accelerator for their support during the test-beam. We also very much appreciate the work of Angelo Gandi, Rui de Oliveira and Antonio Teixeira in the CERN Photomechanical workshops (EST-SM-CI), and Alan Honma and Enrico Chesi, also at CERN, for wire bonding and hybrid design. We are very grateful to Jean-Rene Moser and the Lausanne workshop.

References

[1] F. Anghinolfi *et al* . SCTA - A rad-hard BiCMOS analogue readout ASIC for the ATLAS semiconductor tracker. *IEEE Transactions on Nuclear Sciences 44 (1997) 298.*

[2] J. Christiansen. Requirements to the L0 front–end electronics. *LHCb note, LHCb 99-29 ELEC.*

[3] J. Buytaert. SCTA_VELO User manual. *LHCb note, LHCb 2001-045.*

[4] J. Buytaert *et al* . Measurements of the signal shape of a silicon strip detector with SCTA readout. *LHCb note, LHCb 2000-98 VELO.*

[5] T. Bowcock *et al* . Performance of an irradiated Hamamatsu prototype VELO detector. *LHCb note, LHCb 2001-39 VELO.*

[6] T. Bowcock *et al* . Performance of an irradiated Micron prototype VELO detector. *LHCb note, LHCb 2001-40 VELO.*

[7] G. Casse *et al* . Measurement of the Irradiation Profile at the PS Beam. *LHCb note, LHCb 2001-020.*

[8] LHCb collaboration. LHCb Vertex Locator Technical Design Report. *CERN/LHCC/2001-0011.*

[9] J. E. Moyal. Theory of ionization fluctuations. *Phil. Mag. 46 (1955) 263.*

[10] P. Koppenburg. Simulation of the vertex trigger preprocessor: Effects of noise on L1 performance. *LHCb note, LHCb 1999-03 TRIG.*

[11] S. Saladino. Study of vertex silicon detectors for LHC experiments. *Thesis, CERN-OPEN-99-374.*

[12] P. Riedler. Radiation Damage Effects and Performance of Silicon Strip Detectors using LHC Readout Electronics. *Thesis, CERN-THESIS-2000-002.*

[13] D. Baumeister *et al* . The Beetle Reference Manual. *LHCb note, LHCb 2001-046.*